ChemPubSoc Europe
DOI: 10.1002/chem.201700731
CHEMISTRY A European Journal Concept

Materials Science

High-Throughput Optical Imaging and Spectroscopy of One-Dimensional Materials

Fengrui Yao[+],[a] Cheng Chen[+],[a] Can Liu,[a] Jin Zhang,[b] Feng Wang,[c] and Kaihui Liu*[a]

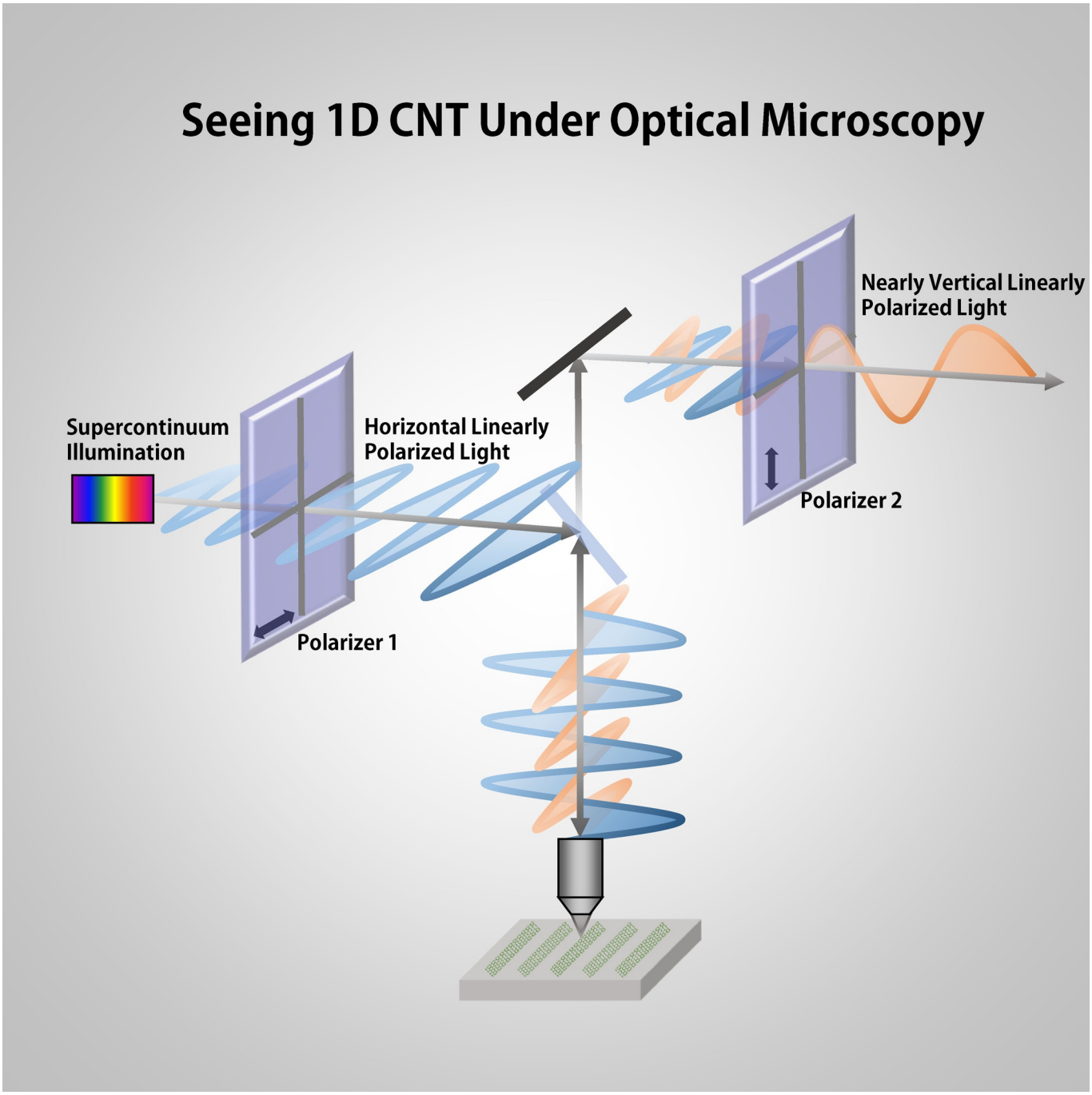

Abstract: Direct visualization of one-dimensional (1D) materials under an optical microscope in ambient conditions is of great significance for their characterizations and applications. However, it is full of challenges to achieve such goal due to their relative small size (ca. 1 nm in diameter) in the optical-diffraction-limited laser spot (ca. 1 μm in diameter). In this Concept article, we introduce a polarization-based optical homodyne detection method that can be used as a general strategy to obtain high-throughput, real-time, optical imaging and in situ spectroscopy of polarization-inhomogeneous 1D materials. We will use carbon nanotubes (CNTs) as an example to demonstrate the applications of such characterization with respect to the absorption signal of individual nanotubes, real-time imaging of individual nanotubes in devices, and statistical structure information of nanotube arrays.

Background

One-dimensional materials (nanotubes, nanowires, nanobelts, nanoribbons and edges or boundaries in two-dimensional materials) have attracted increasing interest owing to their unique structural, electronic, and optical properties.[1–13] For example, 1D carbon nanotubes (CNTs) have been attracting ever-growing attention since their discovery in the early 1990s.[14–30] Based on their unique geometric characteristics and strong 1D anisotropies, 1D nanostructures are believed to play an important role as next-generation building blocks for electronic or optoelectronic devices, for chemical or biological sensors, for energy harvesting, storage and so on.[31–39] Advanced analytical equipment, such as atomic force microscopes (AFM), scanning electron microscopes (SEM) and transmission electron microscopes (TEM), have been employed to study 1D materials.[40–43] However, these techniques suffer from their limitations, like a small operating space, limited accessibility, narrow field of view and/or requiring high vacuum, which restrict their efficiency and applicability.[44] In contrast, optical microscopes and spectroscopy have long been employed to study nanomaterials and have proved to be very efficient.[45–47] A natural limitation, however, comes into play: the diffraction limit makes the focus of light with size around the light wavelength (ca. 1 μm) and the diameter of 1D materials is only in the nm scale, so that great difficulties had been encountered when using those techniques in 1D material research due to the mismatch of these two sizes.

Take CNTs for example, the illumination beam size is several orders of magnitude larger than the diameter of a single CNT (ca. 1 nm), so the typical absorption signal of individual CNT is very small (ca. 10^{-4} to 10^{-5}), which is too weak to be probed under conventional optical microscope, because the signal will be easily blurred by any tiny intensity fluctuations of the light source or environmental fluctuation. To address this challenge, great amount of effort has been undertaken in areas such as fluorescence microscopy,[22,28,48–50] Raman spectroscopy,[51–55] Rayleigh scattering,[56–59] and particle-deposition-assisted optical image.[60–62] However, the preparation of samples and the identification of CNTs are quite complex and time-consuming by these techniques. Different from conventional optical spectroscopy, nano-optical spectroscopy combines new physical theories and experimental techniques to measure small optical signals of low-dimensional materials.[45,63–65] Recently, an optical homodyne detection method has been developed. By using this technique, the amplitude of a carbon nanotube optical signal can be enhanced by two orders of magnitude, which makes it possible to acquire high-throughput optical images and wide-range spectra of a variety of polarization-inhomogeneous nanomaterials in a few seconds.[66] In this concept article, we will summarize the concept of optical homodyne detection, describe the polarization-based homodyne microscope, and discuss its theory and applications (1D CNTs will be used as an example material). It is hoped that this review will provide useful information in the convenient characterization based on homodyne detection, and inspire growing efforts in the area of 1D materials for versatile applications.

Introduction to Homodyne Detection

Theory

Homodyne detection is a method that was originally developed in the field of radio waves and microwaves. It has been extensively exploited as a means of achieving low-cost coherent detection,[67] and a number of sophisticated detection schemes based on the homodyne concept have been studied.[68–70] Till now, a lot of applications of this technique have already been proposed, such as magnetic resonance imaging,[71] optical feedback,[69] measurement of optical phase,[72] and detection of density-matrix.[73] What is more, homodyne detection was one of the key techniques in demonstrating spooky (A single quantum particle can be described by a wavefunction that spreads over arbitrarily large distances; however, it is never detected in two (or more) places. This strange phenomenon is explained in the quantum theory by what Einstein repudiated as "spooky action at a distance": the instantaneous nonlocal collapse of the wavefunction to wherever the particle

[a] *F. Yao,[+] C. Chen,[+] C. Liu, Prof. K. Liu*
State Key Laboratory for Mesoscopic Physics
School of Physics
Collaborative Innovation Center of Quantum Matter
Peking University, Beijing 100871 (P. R. China)
E-mail: khliu@pku.edu.cn

[b] *Prof. J. Zhang*
Center for Nanochemistry
Beijing Science and Engineering Center for Nanocarbons
College of Chemistry and Molecular Engineering
Peking University, Beijing 100871 (P. R. China)

[c] *Prof. F. Wang*
Department of Physics
University of California at Berkeley
Advanced Light Source Division and Materials Sciences Division
Lawrence Berkeley National Laboratory
Berkeley, CA 94720 (USA)

[+] *These authors contributed equally to this paper.*

is detected) action at a distance.[74] In addition, it has long been proposed and investigated as a useful technique to minimize the impact of laser phase noise in optical communication systems.[22]

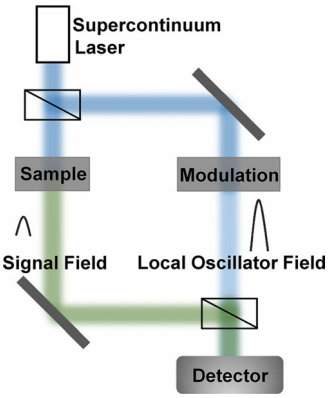

Figure 1. Schematic of optical homodyne detection. A laser is separated into two beams, one to generate signal field and the other to generate local oscillator field. The interference between signal and local oscillator gives out the final detection signal. The separate control of signal and local oscillator can enhance the signal inensity.

For small optical signal measurements, homodyne detection is a kind of optical interferometry, in which a weak signal (E_s) interferes with a relative strong "local oscillator" wave (E_{LO}) (Figure 1). Under each given optical frequency, the detected light intensity change ($\Delta I/I$) is the result of the interference between the signal (E_s) and the local oscillator electric field (E_{LO}) and is given by Equation (1) in which φ is the relative phase between E_s and E_{LO}, the small $|E_s|^2$ term has been ignored.

$$\frac{\Delta I}{I} = \frac{|E_{LO} + E_s|^2 - |E_{LO}|^2}{|E_{LO}|^2} = \frac{2|E_s|}{|E_{LO}|}\cos\varphi \qquad (1)$$

The resulting mixed modulation signal ($\Delta I/I$) that carries the information (amplitude, phase) of the original desired signal is then detected. In this way, the amplitude of the mixing signal ($|E_s|/|E_{LO}|$) measured by homodyne detection can be greatly enhanced to an easily detectable level if one can separately control the magnitude of E_s and E_{LO} and make $|E_s|/|E_{LO}|$ larger.

Polarization-based homodyne system

One example of an optical homodyne detection technique is high-throughput polarization-based homodyne microscopy in a transmission configuration (Figure 2 a). In this setup, the scattered light wave from an individual CNT interferes with the transmitted light, and the detected modulation singal ($\Delta I/I$) originates from the interference between the nanotube forward scattering wave (E_{NT}) and the unperturbed incident light (E_{in}), then Equation (1) will be transformed into Equation (2), in which α is the nanotube absorption, and φ denotes the phase difference between E_{NT} and E_{in} at the detector.

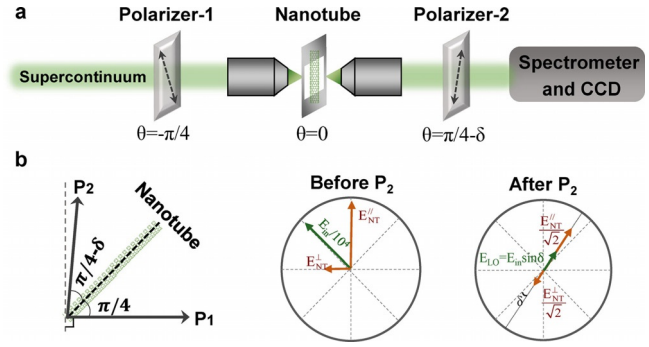

Figure 2. High-throughput polarization-based homodyne microscopy in a transmission configuration. a) Polarization of supercontinuum laser is controlled by two nearly $\pi/2$ crossed polarizers (with a small deviation angle δ). Suspended individual nanotubes are positioned at the focus of the two confocal objectives and with an angle of $\pi/4$ with respect to polarizer 1. b) The transmitted light (E_{in}) interferes with the weak nanotube signal (E_{NT}). After polarizer 2, dramatic reduction of the transmission electrical field ($E_{LO}=E_{in}\sin\delta$) and little loss of nanotubes [$E_s = (E_{NT}^{\parallel} - E_{NT}^{\perp})/\sqrt{2}$] result in the greatly enhanced homodyne signal. The signal ($\Delta I/I$) is enhanced by about two orders of magnitude, reaching approximately a 1% level. Reprinted with permission from reference [58]. (Copyright 2014 National Academy of Sciences).

$$\frac{\Delta T}{T} = \frac{2|E_{NT}|}{|E_{in}|}\cos\varphi = -\alpha \qquad (2)$$

As discussed above, homodyne detection can enormously increase the detected signal intensity. From Equation (2) we can see that the signal could be enlarged by reducing the local oscillator electric field (E_{in}), while maintaining the signal (E_{NT}). Based on this idea, the polarization manipulation method has been applied, which utilizes the strong depolarization effect of 1D CNTs. As shown in Figure 2 a, two nearly $\pi/2$ crossed polarizers (with a small deviation angle δ) are used to control the polarization direction of incident and outgoing light, and two polarization-maintaining objectives are placed confocally between this polarizer pair. Broadband supercontinuum illumination is used to ensure wide-range and high-throughput spectra. The CNTs are positioned at the focus of the two objectives, at $\pi/4$ with respect to the first polarizer; its position can be controlled to move in and out of focus center of laser by a high precision piezo stage. A spectrometer equipped with a linear-array charge-coupled device (CCD) is used to achieve real-time signal acquisition. Theoretically, after the second polarizer we can use Equations (3) and (4) in which $E_{NT}^{\parallel}$ and $E_{NT}^{\perp}$ are nanotube field along and perpendicular to the nanotube axis, respectively.

$$E_{LO} = E_{in}\sin\delta \qquad (3)$$

$$E_s = \frac{E_{NT}^{\parallel} - E_{NT}^{\perp}}{\sqrt{2}} \qquad (4)$$

Considering E_{LO}: $E_{in} \approx 10^2$ and E_s: $E_{NT} \approx \sqrt{2}$ with a suitable polarizer setting, we find that the nanotube contrast can be enhanced by about two orders of magnitude by using substitute E_{Lo} and E_s [from Eqs. (3) and (4)] in Equation (1). With a small δ,

the greatly enhanced optical contrast $\Delta I/I$ can reach about a 1% level (compared with 10^{-4} in conventional transmission methods) and becomes easily detectable.[66]

Practical Applications

Probing the absorption cross-section of suspended CNTs

Optical absorption is one of the fundamental parameters to characterize CNTs linear optical properties and many other parameters, such as absorption coefficient, scattering coefficient, dielectric coefficient and refractive index, can be derived from it.[66] Especially, information about the absorption cross-section of individual CNT is of great interest for its importance in understanding their electronic structures, in evaluating quantum efficiency of their photoluminescence[22,75] and photocurrent,[76–78] also in investigating the unique many-body effects in 1D systems.[79–84] What is more, the absorption cross-section is also a bridge connecting CNTs properties and theory because it can be given directly by theoretical calculations. However, the weak signal of CNTs often submerges in the background signal and laser intensity fluctuations, making the measurements very difficult. Therefore, previous absorption measurements on ensemble CNTs samples only give information about averaged behavior[85–87] and recent absorption studies of individual CNTs cannot determine the absolute absorption cross section effectively over a wide spectral range.[82,88–90]

However, with the aid of the homodyne microscopy of transmission configuration mentioned above, we can get high-throughput optical contrast spectra of single CNTs, and derive the absorption cross-section from it by knowing the laser spot profile (Figure 3 a and b). It is the first time that the absorption cross-section of many individual CNTs could be quantitatively determined over broad spectral range in a short time. With such a data base in hand, it is now possible to establish an important structure-absorption map of different nanotube species.[91]

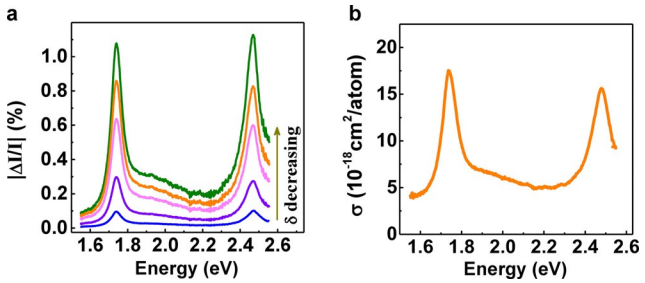

Figure 3. CNT absorption spectra. a) Absorption spectra of a suspended CNT, the optical contrast is enlarged when the deviation angle δ decreases. b) Absorption cross-section of the same CNT derived by its absorption spectra. Reprinted with permission from reference [58]. (Copyright 2014 National Academy of Sciences).

In-situ imaging and spectroscopy of individual CNT

It should be noted that the homodyne detection configuration mentioned above is based on suspended CNTs. However, for its real applications, such as in nano-electronics and optoelectronics, real-time optical imaging of CNTs on devices is desperately in need, which is more challenging than that of suspended CNTs, because the signal scattered by CNTs is nearly three orders of magnitude smaller than that reflected by substrate, generally. Based on the same homodyne detection concept mentioned above, a polarization-based optical microscope in the reflection configuration has been successfully constructed and high-throughput optical imaging and in situ spectroscopy of individual CNTs in devices has been realized.[92]

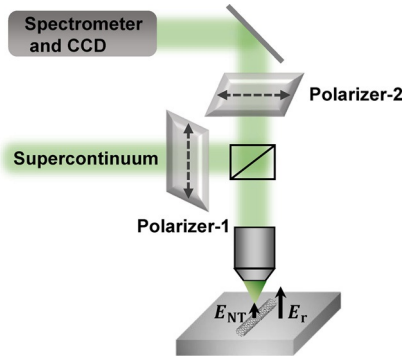

Figure 4. High-throughput polarization-based homodyne microscopy in reflection configuration. Horizontally polarized incident light (after polarizer 1) illuminates a nanotube oriented at $\pi/4$. Polarizer 2 is oriented close to the vertical direction (with a small angle deviation δ), which strongly reduces the reflection field, but only slightly decreases the nanotube-scattered field, resulting in greatly enhanced homodyne signal. Reprinted with permission from reference [83]. (Copyright 2013 Nature Publishing Group).

As shown in Figure 4, similar to the transmission configuration, two nearly $\pi/2$ perpendicular polarizers and one reflective microscope objectives are used, and the CNT is also oriented at $\pi/4$ relative to the first polarization direction. By controlling the stage movement back and forth with respect to the laser light, the objective collects the nanotube-scattered (E_{NT}) and the bare substrate-reflected (E_r) light, respectively (Figure 4). Then, the optical contrast of a CNT in a reflection configuration can be derived from interference between the nanotube-scattered electric field E_{NT} and the substrate-reflected electric field E_r at the detector, as given by Equation (5) below, in which R is the optical signal from pure substrate reflection, ΔR is the optical signal difference arising from the presence of a nanotube, and ϕ denotes the phase difference between E_{NT} and E_r at the detector.

$$\frac{\Delta R}{R} = \frac{|E_r + E_{NT}|^2 - |E_r|^2}{|E_r|^2} = \frac{2|E_{NT}|}{|E_r|}\cos\phi \qquad (5)$$

By manipulating the polarization, similar to the transmission configuration, this method could strongly reduce the reflection field E_r, but largely keep the nanotube field at E_{NT}, so that the

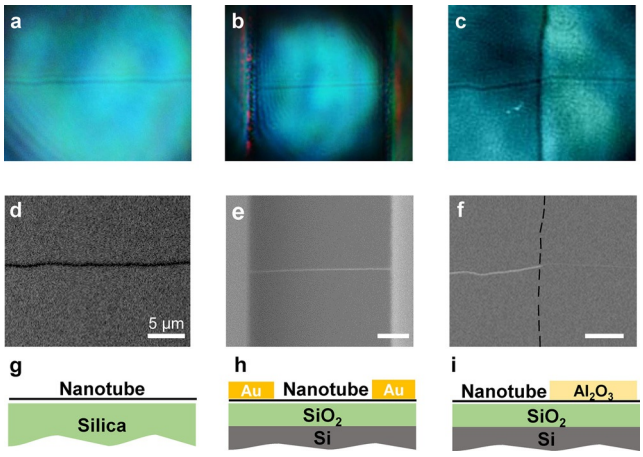

Figure 5. Real-time optical imaging of individual CNTs on substrate or in device. Direct optical images of the individual nanotubes a) on a fused-silica, b) in a back-gated field-effect transistor device (with two gold electrodes), c) located partly under an Al_2O_3 dielectric layer, with an integration time of about 20 ms. d)–f) Scanning electron microscopy images of the nanotubes corresponding to the optical images in a)–c). The invisible Al_2O_3 edge in f) is indicated by the dashed line. g)–i) Schematics of nanotubes corresponding to the optical images in a)–c). Reprinted with permission from reference [83]. (Copyright 2013 Nature Publishing Group).

optical contrast is sufficiently enhanced. Here E_r works as the local oscillator.

Based on this technique, direct imaging of a single CNT has been realized in diverse conditions, for example, CNTs on a fused-silica substrate (Figure 5a), in a back-gated field-effect transistor with source-drain electrodes (Figure 5b), and partly covered by an Al_2O_3 dielectric layer (Figure 5c). Corresponding scanning electron micrographs and schematics of a nanotube are presented in Figure 5d–i. As shown in these figures, the contrast is efficiently enlarged to about 1% level by the above method so that we can easily observe individual CNTs merely by optical microscopy rather than electron microscopy. Because of its versatility, this technique can be potentially applied in different ways, such as feeding back to the growth, monitoring device performances, sensing bio-systems, and studying the in situ growth of nanotube materials.

More importantly, optical absorption spectra of a single CNT can be acquired in situ and its chirality can be determined accurately with the aid of an experimental transition-chirality atlas (Figure 6a–c). Thus, this method can achieve high-throughput determination of CNT chirality distribution on diverse substrates and in situ characterization of its electronic structure in operating devices, which may lead to the realization of two major goals in central CNT research: achieving chiral-selective growth and understanding chiral-dependent device physics. Such characterization also helps the control over the location and orientation of the produced nanotubes on substrate.[93–96] In addition, the mechanism of formation of a single CNT has been widely discussed; however, up to now, this subject is still controversial.[97–100] Such a technique can be developed further to understand the dynamic processes of nanotube growth at 20 ms time scale and there is hope that dispute may be resolved.

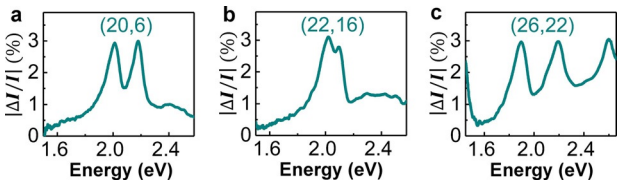

Figure 6. In-situ optical spectra of individual nanotubes. a) on a fused-silica, b) in a back-gated field-effect transistor device (with two gold electrodes), c) under an Al_2O_3 dielectric layer. We can identify chiralities of these nanotubes as (20, 6), (22, 16) and (26, 22), respectively. Reprinted with permission from reference [83]. (Copyright 2013 Nature Publishing Group).

Optical imaging and statistical information of horizontal CNT arrays

In fact, the homodyne detection method is also applicable for imaging horizontal CNT arrays on diverse substrates.[101] The principle is similar to that of individual CNT measurements in the above-mentioned reflection configuration. A schematic configuration of polarization microscopy for carbon nanotube arrays is shown in Figure 7a and the concept of reflection optical contrast in Figure 7b. Optical images of CNT arrays can be obtained on different substrates, for example, on quartz (Figure 7c), fused silica (Figure 7d), and SiO_2/Si with electrodes (Figure 7e); immersed in different aqueous solution (Figure 7f) and oil (Figure 7g); and even under high temperature of 900 °C (Figure 7h). In addition, high-throughput determination of statistical structure information for horizontal CNT arrays on diverse substrates have also been obtained.[101]

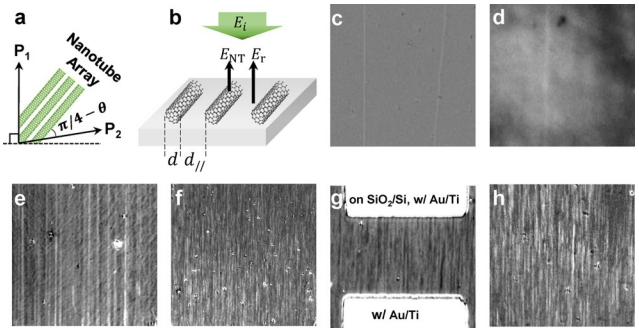

Figure 7. Optical images of CNT arrays. a) Schematic configuration of polarization microscopy with CNT arrays. b) Schematic concept of reflection optical contrast for CNT arrays. c) CNT arrays on fused silica, d) on quartz, e) on SiO_2/Si substrates with electrodes, f) in water, g) in oil, and h) under 900 °C in argon gas. Reprinted with permission from reference [92]. (Copyright 2015 John Wiley and Sons).

Firstly, from their integral optical contrast in an optical image, the line density of CNT arrays can be determined. For horizontally aligned CNT arrays, for example, on transparent substrates, the optical reflection contrast ($\Delta R/R$) is directly related to the absorption in a linear way by Equation (6) in which n_s is the refractive index of the substrate, and A is the optical absorption.

$$\frac{\Delta R}{R}=\frac{|E_r+E_{NT}|^2-|E_r|^2}{|E_r|^2}=\frac{2|E_{NT}|}{|E_r|}\cos\phi=\frac{4}{n_s^2-1}A \quad (6)$$

According to the approximation sum rule, the integrated absorption per atom in a wide spectral range is nearly the same for all graphitic materials, so the CNT array line density can be directly obtained by averaging the integral absorption, as given by Equation (7) in which I, A, $\bar{d}$, s_0, σ are the CNTs line density, absorption, mean diameter, areal in-plane atom density, and the absorption cross-section per atom, respectively.

$$I=\frac{A}{\pi\bar{d}s_0\sigma} \quad (7)$$

Since s_0 is of constant value, σ could be systematically obtained by transmission homodyne detection, as proposed above,[66] and the mean diameter $\bar{d}$ can be determined by Raman spectroscopy from the radial breathing mode (RBM) vibrations.[102]

With all the information above, from the optical absorption, the CNT line density can be obtained directly. As shown in Figure 8, the ability in determining the line density by using

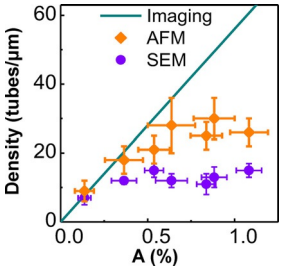

Figure 8. The comparison between SEM, AFM, and optical imaging method in determining the line density. SEM and AFM methods become invalid for line density exceeding about 10 and 30 tubes per μm, respectively. Reprinted with permission from reference [92]. (Copyright 2015 John Wiley and Sons).

SEM, AFM, and optical imaging methods has been compared. The maximum line density can be reliably determined by optical imaging as large as 50 tubes per μm, while SEM and AFM fails to give out the right value in such high density, which clearly demonstrates the superiority of this optical method. Secondly, the M/S ratio (metal-to-semiconductor ratio) of CNT arrays can be determined from their color-resolved optical contrast in the optical image. A different optical transition peak position means a different color for metallic or semiconducting CNTs, and this information can be seen in the Kataura plot (Figure 9a), which shows the relation between the optical transition energy E_{ij} and the nanotube diameter—this plot was generated from the experimental atlas of nanotube optical transitions.[84] Therefore, in principle the M/S ratio can be determined by evaluating the optical contrast ratio between different color regions.

Technically, the reflection light of the CNTs on substrate R_{CNT} and on bare substrate (R_s) can be measured by averaging the image brightness of every single pixel for the regions of interest (ROI) by using Equation (8) in which E_i is the bandwidth (in energy) for the specific filter used in imaging. By evaluating the optical contrast ratio between different color regions in the optical image, the M/S ratio can be obtained.

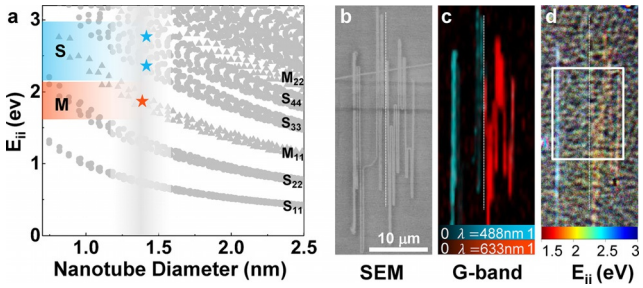

Figure 9. Determination of the M/S ratio for CNT array by colour-resolved optical contrast. a) The Kataura plot generated from the experimental atlas of nanotube optical transitions. The vertical grey bar shows the diameter region of our as-grown nanotube arrays. b)–d) SEM, Raman G-mode mapping and optical image of a "U"-shaped hetero-nanotube array on quartz, respectively. The vertical dashed lines indicate the boundary positions for the two types of nanotubes. Reprinted with permission from reference [92]. (Copyright 2015 John Wiley and Sons).

$$\text{Integral optical contrast}=\frac{\sum\left(\frac{R_{CNT}-R_S}{R_S}\right)E_i}{\sum E_i} \quad (8)$$

For example, a special "U"-shaped hetero-nanotube sample (Figure 9b) was observed by color-resolved optical contrast. The vertical dashed line in the Raman G-mode mapping shows the boundary between the two types (Figure 9c). Using the integral optical contrast of the two regions as separated by the dashed line and outlined by the white box in Figure 9d, the line density is 0.71 tubes per μm for the S nanotubes on the left and 0.77 tubes per μm for the M nanotubes on the right, giving an M/S ratio is 1.08. This method can work well even when CNTs are tightly packed as a continuous film. It has evident superiority compared with traditional optical techniques restricted by the diffraction limit (the resolution of which is lower than ca.1 tube per μm).

Summary and Outlook

In this article, we described the concept of a polarization-based homodyne detection method, based on which, the amplitude of single CNT signal is enhanced by two orders of magnitude. Polarization-based homodyne microscopy has been developed by using the transmission and reflection configurations. Thus, high-throughput optical imaging and spectroscopy of individual CNTs and horizontal CNT arrays have been realized. These techniques have been used for studying CNTs in devices and on diverse substrates, and for probing the absorption cross-section of individual CNTs and statistical structure information of CNT arrays. Such a development will accelerate the controllable growth of CNTs with high density and high semiconducting purity, and further enhance the understanding of physics in CNTs and contribute to their application in nano-

technology eventually. Clearly, this technique is not limited to CNTs, but establishes a general analytical means for the entire class of 1D materials with polarization inhomogeneity. Such techniques can also be extended to quasi-1D materials, like muscle fibers, DNA long chain, boundaries of 2D materials. There is no doubt that this technique has plenty of potential applications in fast characterization and in situ monitoring of 1D nanostructures when applied in the fields of electronics and biology.

Acknowledgements

We acknowledge the financial support from National Key R&D Program of China (2016YFA0300903), National Natural Science Foundation of China (NSFC) (11474006, 51522201 and 91433102) and the National Program for Thousand Young Talents of China, and National Science Foundation (NSF) (DMR-1404865).

Conflict of interest

The authors declare no conflict of interest.

Keywords: carbon nanotubes · optical imaging · homodyne detection · materials science · one-dimensional materials · polarization microscopy

[1] S. Iijima, *Nature* **1991**, *354*, 56 – 58.
[2] S. Iijima, T. Ichihashi, *Nature* **1993**, *363*, 603 – 605.
[3] A. M. Morales, C. M. Lieber, *Science* **1998**, *279*, 208 – 211.
[4] M. H. Huang, Y. Y. Wu, H. Feick, N. Tran, E. Weber, P. D. Yang, *Adv. Mater.* **2001**, *13*, 113 – 116.
[5] M. H. Huang, S. Mao, H. Feick, H. Q. Yan, Y. Y. Wu, H. Kind, E. Weber, R. Russo, P. D. Yang, *Science* **2001**, *292*, 1897 – 1899.
[6] Z. W. Pan, Z. R. Dai, Z. L. Wang, *Science* **2001**, *291*, 1947 – 1949.
[7] M. S. Gudiksen, L. J. Lauhon, J. Wang, D. C. Smith, C. M. Lieber, *Nature* **2002**, *415*, 617 – 620.
[8] Y. N. Xia, P. D. Yang, Y. G. Sun, Y. Y. Wu, B. Mayers, B. Gates, Y. D. Yin, F. Kim, Y. Q. Yan, *Adv. Mater.* **2003**, *15*, 353 – 389.
[9] P. X. Gao, Y. Ding, W. J. Mai, W. L. Hughes, C. S. Lao, Z. L. Wang, *Science* **2005**, *309*, 1700 – 1704.
[10] H.-W. Liang, S. Liu, S.-H. Yu, *Adv. Mater.* **2010**, *22*, 3925 – 3937.
[11] V. V. Deshpande, M. Bockrath, L. I. Glazman, A. Yacoby, *Nature* **2010**, *464*, 209 – 216.
[12] A. M. van der Zande, P. Y. Huang, D. A. Chenet, T. C. Berkelbach, Y. M. You, G. H. Lee, T. F. Heinz, D. R. Reichman, D. A. Muller, J. C. Hone, *Nat. Mater.* **2013**, *12*, 554 – 561.
[13] C. G. Tao, L. Y. Jiao, O. V. Yazyev, Y. C. Chen, J. J. Feng, X. W. Zhang, R. B. Capaz, J. M. Tour, A. Zettl, S. G. Louie, H. J. Dai, M. F. Crommie, *Nat. Phys.* **2011**, *7*, 616 – 620.
[14] T. W. Ebbesen, H. J. Lezec, H. Hiura, J. W. Bennett, H. F. Ghaemi, T. Thio, *Nature* **1996**, *382*, 54 – 56.
[15] M. M. J. Treacy, T. W. Ebbesen, J. M. Gibson, *Nature* **1996**, *381*, 678 – 680.
[16] A. Thess, R. Lee, P. Nikolaev, H. J. Dai, P. Petit, J. Robert, C. H. Xu, Y. H. Lee, S. G. Kim, A. G. Rinzler, D. T. Colbert, G. E. Scuseria, D. Tomanek, J. E. Fischer, R. E. Smalley, *Science* **1996**, *273*, 483 – 487.
[17] M. Bockrath, D. H. Cobden, P. L. McEuen, N. G. Chopra, A. Zettl, A. Thess, R. E. Smalley, *Science* **1997**, *275*, 1922 – 1925.
[18] S. J. Tans, M. H. Devoret, H. J. Dai, A. Thess, R. E. Smalley, L. J. Geerligs, C. Dekker, *Nature* **1997**, *386*, 474 – 477.
[19] T. W. Odom, J. L. Huang, P. Kim, C. M. Lieber, *Nature* **1998**, *391*, 62 – 64.
[20] M. Bockrath, D. H. Cobden, J. Lu, A. G. Rinzler, R. E. Smalley, L. Balents, P. L. McEuen, *Nature* **1999**, *397*, 598 – 601.
[21] T. W. Odom, J. L. Huang, C. L. Cheung, C. M. Lieber, *Science* **2000**, *290*, 1549 – 1552.
[22] S. M. Bachilo, M. S. Strano, C. Kittrell, R. H. Hauge, R. E. Smalley, R. B. Weisman, *Science* **2002**, *298*, 2361 – 2366.
[23] N. M. Gabor, Z. Zhong, K. Bosnick, J. Park, P. L. McEuen, *Science* **2009**, *325*, 1367 – 1371.
[24] Z. K. Tang, L. Y. Zhang, N. Wang, X. X. Zhang, G. H. Wen, G. D. Li, J. N. Wang, C. T. Chan, P. Sheng, *Science* **2001**, *292*, 2462 – 2465.
[25] H. Ishii, H. Kataura, H. Shiozawa, H. Yoshioka, H. Otsubo, Y. Takayama, T. Miyahara, S. Suzuki, Y. Achiba, M. Nakatake, T. Narimura, M. Higashiguchi, K. Shimada, H. Namatame, M. Taniguchi, *Nature* **2003**, *426*, 540 – 544.
[26] P. Jarillo-Herrero, J. A. van Dam, L. P. Kouwenhoven, *Nature* **2006**, *439*, 953 – 956.
[27] A. Javey, J. Guo, Q. Wang, M. Lundstrom, H. J. Dai, *Nature* **2003**, *424*, 654 – 657.
[28] M. J. O'Connell, S. M. Bachilo, C. B. Huffman, V. C. Moore, M. S. Strano, E. H. Haroz, K. L. Rialon, P. J. Boul, W. H. Noon, C. Kittrell, J. P. Ma, R. H. Hauge, R. B. Weisman, R. E. Smalley, *Science* **2002**, *297*, 593 – 596.
[29] F. Wang, G. Dukovic, L. E. Brus, T. F. Heinz, *Science* **2005**, *308*, 838 – 841.
[30] J. Chen, V. Perebeinos, M. Freitag, J. Tsang, Q. Fu, J. Liu, P. Avouris, *Science* **2005**, *310*, 1171 – 1174.
[31] X. F. Duan, Y. Huang, Y. Cui, J. F. Wang, C. M. Lieber, *Nature* **2001**, *409*, 66 – 69.
[32] Y. Cui, Q. Q. Wei, H. K. Park, C. M. Lieber, *Science* **2001**, *293*, 1289 – 1292.
[33] Y. Cui, C. M. Lieber, *Science* **2001**, *291*, 851 – 853.
[34] Y. Li, F. Qian, J. Xiang, C. M. Lieber, *Materials Today* **2006**, *9*, 18 – 27.
[35] P. Avouris, Z. H. Chen, V. Perebeinos, *Nat. Nanotechnol.* **2007**, *2*, 605 – 615.
[36] P. Avouris, M. Freitag, V. Perebeinos, *Nat. Photonics* **2008**, *2*, 341 – 350.
[37] A. Fujishima, K. Honda, *Nature* **1972**, *238*, 37.
[38] S. B. Desai, S. R. Madhvapathy, A. B. Sachid, J. P. Llinas, Q. X. Wang, G. H. Ahn, G. Pitner, M. J. Kim, J. Bokor, C. M. Hu, H. S. P. Wong, A. Javey, *Science* **2016**, *354*, 99 – 102.
[39] C. Qiu, Z. Zhang, M. Xiao, Y. Yang, D. Zhong, L. Peng, *Science* **2017**, *355*, 271 – 276.
[40] M. F. Yu, M. J. Dyer, G. D. Skidmore, H. W. Rohrs, X. K. Lu, K. D. Ausman, J. R. Von Ehr, R. S. Ruoff, *Nanotechnology* **1999**, *10*, 244 – 252.
[41] C. Thelander, L. Samuelson, *Nanotechnology* **2002**, *13*, 108 – 113.
[42] H. F. Yang, F. H. Li, C. S. Shan, D. X. Han, Q. X. Zhang, L. Niu, A. Ivaska, *J. Mater. Chem.* **2009**, *19*, 4632 – 4638.
[43] H. K. He, C. Gao, *Chem. Mater.* **2010**, *22*, 5054 – 5064.
[44] R. Zhang, Y. Zhang, Q. Zhang, H. Xie, H. Wang, J. Nie, Q. Wen, F. Wei, *Nat. Commun.* **2013**, *4*, 1727 – 1735.
[45] J. N. Chen, M. Badioli, P. Alonso-Gonzalez, S. Thongrattanasiri, F. Huth, J. Osmond, M. Spasenovic, A. Centeno, A. Pesquera, P. Godignon, A. Z. Elorza, N. Camara, F. J. G. de Abajo, R. Hillenbrand, F. H. L. Koppens, *Nature* **2012**, *487*, 77 – 81.
[46] A. Albanese, A. K. Lam, E. A. Sykes, J. V. Rocheleau, W. C. Chan, *Nat. Commun.* **2013**, *4*, 2718.
[47] D. J. Late, Y. K. Huang, B. Liu, J. Acharya, S. N. Shirodkar, J. J. Luo, A. M. Yan, D. Charles, U. V. Waghmare, V. P. Dravid, C. N. R. Rao, *Acs Nano* **2013**, *7*, 4879 – 4891.
[48] S. Chaudhary, J. H. Kim, K. V. Singh, M. Ozkan, *Nano Lett.* **2004**, *4*, 2415 – 2419.
[49] V. V. Didenko, V. C. Moore, D. S. Baskin, R. E. Smalley, *Nano Lett.* **2005**, *5*, 1563 – 1567.
[50] R. Duggal, M. Pasquali, *Phys. Rev. Lett.* **2006**, *96*, 246104.
[51] A. M. Rao, E. Richter, S. Bandow, B. Chase, P. C. Eklund, K. A. Williams, S. Fang, K. R. Subbaswamy, M. Menon, A. Thess, R. E. Smalley, G. Dresselhaus, M. S. Dresselhaus, *Science* **1997**, *275*, 187 – 191.
[52] M. Zheng, A. Jagota, M. S. Strano, A. P. Santos, P. Barone, S. G. Chou, B. A. Diner, M. S. Dresselhaus, R. S. McLean, G. B. Onoa, G. G. Samsonidze, E. D. Semke, M. Usrey, D. J. Walls, *Science* **2003**, *302*, 1545 – 1548.
[53] R. Krupke, F. Hennrich, H. von Lohneysen, M. M. Kappes, *Science* **2003**, *301*, 344 – 347.
[54] M. S. Dresselhaus, G. Dresselhaus, R. Saito, A. Jorio, *Phys. Rep.* **2005**, *409*, 47 – 99.

[55] M. S. Dresselhaus, A. Jorio, M. Hofmann, G. Dresselhaus, R. Saito, *Nano Lett.* **2010**, *10*, 751 – 758.
[56] M. Y. Sfeir, F. Wang, L. M. Huang, C. C. Chuang, J. Hone, S. P. O'Brien, T. F. Heinz, L. E. Brus, *Science* **2004**, *306*, 1540 – 1543.
[57] F. Wang, M. Y. Sfeir, L. M. Huang, X. M. H. Huang, Y. Wu, J. H. Kim, J. Hone, S. O'Brien, L. E. Brus, T. F. Heinz, *Phys. Rev. Lett.* **2006**, *96*, 167401.
[58] D. Y. Joh, L. H. Herman, S. Y. Ju, J. Kinder, M. A. Segal, J. N. Johnson, G. K. Chan, J. Park, *Nano Lett.* **2011**, *11*, 1 – 7.
[59] W. Wu, J. Yue, X. Lin, D. Li, F. Zhu, X. Yin, J. Zhu, J. Wang, J. Zhang, Y. Chen, X. Wang, T. Li, Y. He, X. Dai, P. Liu, Y. Wei, J. Wang, W. Zhang, Y. Huang, L. Fan, L. Zhang, Q. Li, S. Fan, K. Jiang, *Nano Res.* **2015**, *8*, 2721 – 2732.
[60] S. M. Huang, Y. Qian, J. Y. Chen, Q. R. Cai, L. Wan, S. Wang, W. B. Hu, *J. Am. Chem. Soc.* **2008**, *130*, 11860 – 11861.
[61] H. B. Chu, R. L. Cui, J. Y. Wang, J. A. Yang, Y. Li, *Carbon* **2011**, *49*, 1182 – 1188.
[62] J. Wang, T. Li, B. Xia, X. Jin, H. Wei, W. Wu, Y. Wei, J. Wang, P. Liu, L. Zhang, Q. Li, S. Fan, K. Jiang, *Nano Lett.* **2014**, *14*, 3527 – 3533.
[63] A. V. Zayats, I. I. Smolyaninov, A. A. Maradudin, *Phys. Rep.* **2005**, *408*, 131 – 314.
[64] S. Lal, S. Link, N. J. Halas, *Nat. Photonics* **2007**, *1*, 641 – 648.
[65] L. Luo, I. Chatzakis, A. Patz, J. G. Wang, *Phys. Rev. Lett.* **2015**, *114*, 107402.
[66] K. Liu, X. Hong, S. Choi, C. Jina, R. Capaza, J. Kima, W. Wange, X. Baie, S. Louie, E. Wang, F. Wang, *Proc. Natl. Acad. Sci. USA* **2014**, *111*, 7564 – 7569.
[67] R. S. Luis, B. J. Puttnam, J. M. D. Mendinueta, S. Shinada, M. Nakamura, Y. Kamio, N. Wada, *IEEE Photonics Technol. Lett.* **2015**, *27*, 608 – 611.
[68] H. P. Yuen, V. W. S. Chan, *Opt. Lett.* **1983**, *8*, 177 – 179.
[69] H. M. Wiseman, G. J. Milburn, *Phys. Rev. Lett.* **1993**, *70*, 548 – 551.
[70] E. Ip, A. P. T. Lau, D. J. F. Barros, J. M. Kahn, *Opt. Express* **2008**, *16*, 753 – 791.
[71] D. C. Noll, D. G. Nishimura, A. Macovski, *IEEE Trans. Med. Imaging* **1991**, *10*, 154 – 163.
[72] M. A. Armen, J. K. Au, J. K. Stockton, A. C. Doherty, H. Mabuchi, *Phys. Rev. Lett.* **2002**, *89*, 133602.
[73] G. M. D'Ariano, C. Macchiavello, M. G. A. Paris, *Phys. Rev. A* **1994**, *50*, 4298 – 4302.
[74] M. Fuwa, S. Takeda, M. Zwierz, H. M. Wiseman, A. Furusawa, *Nat. Commun.* **2015**, *6*, 6665 – 6670.
[75] J. Lefebvre, P. Finnie, *Phys. Rev. Lett.* **2007**, *98*, 167406.
[76] M. Freitag, Y. Martin, J. A. Misewich, R. Martel, P. H. Avouris, *Nano Lett.* **2003**, *3*, 1067 – 1071.
[77] C. M. Aguirre, S. Auvray, S. Pigeon, R. Izquierdo, P. Desjardins, R. Martel, *Appl. Phys. Lett.* **2006**, *88*, 183104.
[78] F. L. Wang, S. Wang, F. R. Yao, H. T. Xu, N. Wei, K. H. Liu, L. M. Peng, *ACS Nano* **2016**, *10*, 9595 – 9601.
[79] C. D. Spataru, S. Ismail-Beigi, L. X. Benedict, S. G. Louie, *Phys. Rev. Lett.* **2004**, *92*, 077402.
[80] V. Perebeinos, J. Tersoff, P. Avouris, *Phys. Rev. Lett.* **2004**, *92*, 257402.
[81] C. L. Kane, E. J. Mele, *Phys. Rev. Lett.* **2004**, *93*, 197402.
[82] F. Wang, D. J. Cho, B. Kessler, J. Deslippe, P. J. Schuck, S. G. Louie, A. Zettl, T. F. Heinz, Y. R. Shen, *Phys. Rev. Lett.* **2007**, *99*, 227401.
[83] E. Malic, J. Maultzsch, S. Reich, A. Knorr, *Phys. Rev. B* **2010**, *82*, 035433.
[84] K. Liu, J. Deslippe, F. Xiao, R. B. Capaz, X. Hong, S. Aloni, A. Zettl, W. Wang, X. Bai, S. G. Louie, E. Wang, F. Wang, *Nat. Nanotechnol.* **2012**, *7*, 325 – 329.
[85] M. F. Islam, D. E. Milkie, C. L. Kane, A. G. Yodh, J. M. Kikkawa, *Phys. Rev. Lett.* **2004**, *93*, 037404.
[86] Y. Murakami, E. Einarsson, T. Edamura, S. Maruyama, *Phys. Rev. Lett.* **2005**, *94*, 087402.
[87] F. Vialla, C. Roquelet, B. Langlois, G. Delport, S. M. Santos, E. Deleporte, P. Roussignol, C. Delalande, C. Voisin, J. S. Lauret, *Phys. Rev. Lett.* **2013**, *111*, 137402.
[88] S. Berciaud, L. Cognet, P. Poulin, R. B. Weisman, B. Lounis, *Nano Lett.* **2007**, *7*, 1203 – 1207.
[89] L. H. Herman, C. J. Kim, Z. H. Wang, M. H. Jo, J. Park, *Appl. Phys. Lett.* **2012**, *101*, 123102.
[90] J. C. Blancon, M. Paillet, H. N. Tran, X. T. Than, S. A. Guebrou, A. Ayari, A. San Miguel, N. M. Phan, A. A. Zahab, J. L. Sauvajol, N. Del Fatti, F. Vallee, *Nat. Commun.* **2013**, *4*, 2542.
[91] H. Lin, J. Lagoute, V. Repain, C. Chacon, Y. Girard, J. S. Lauret, F. Ducastelle, A. Loiseau, S. Rousset, *Nat. Mater.* **2010**, *9*, 235 – 238.
[92] K. Liu, X. Hong, Q. Zhou, C. Jin, J. Li, W. Zhou, J. Liu, E. Wang, A. Zettl, F. Wang, *Nat. Nanotechnol.* **2013**, *8*, 917 – 922.
[93] J. Kong, H. T. Soh, A. M. Cassell, C. F. Quate, H. J. Dai, *Nature* **1998**, *395*, 878 – 881.
[94] S. S. Fan, M. G. Chapline, N. R. Franklin, T. W. Tombler, A. M. Cassell, H. J. Dai, *Science* **1999**, *283*, 512 – 514.
[95] J. Liu, M. J. Casavant, M. Cox, D. A. Walters, P. Boul, W. Lu, A. J. Rimberg, K. A. Smith, D. T. Colbert, R. E. Smalley, *Chem. Phys. Lett.* **1999**, *303*, 125 – 129.
[96] B. Vigolo, A. Penicaud, C. Coulon, C. Sauder, R. Pailler, C. Journet, P. Bernier, P. Poulin, *Science* **2000**, *290*, 1331 – 1334.
[97] S. Iijima, P. M. Ajayan, T. Ichihashi, *Phys. Rev. Lett.* **1992**, *69*, 3100 – 3103.
[98] S. Amelinckx, X. B. Zhang, D. Bernaerts, X. F. Zhang, V. Ivanov, J. B. Nagy, *Science* **1994**, *265*, 635 – 639.
[99] Y. H. Tang, P. Zhang, P. S. Kim, T. K. Sham, Y. F. Hu, X. H. Sun, N. B. Wong, M. K. Fung, Y. F. Zheng, C. S. Lee, S. T. Lee, *Appl. Phys. Lett.* **2001**, *79*, 3773 – 3775.
[100] L. M. Viculis, J. J. Mack, R. B. Kaner, *Science* **2003**, *299*, 1361 – 1361.
[101] S. Deng, J. Tang, L. Kang, Y. Hu, F. Yao, Q. Zhao, S. Zhang, K. Liu, J. Zhang, *Adv. Mater.* **2016**, *28*, 2018 – 2023.
[102] A. Jorio, R. Saito, J. H. Hafner, C. M. Lieber, M. Hunter, T. McClure, G. Dresselhaus, M. S. Dresselhaus, *Phys. Rev. Lett.* **2001**, *86*, 1118 – 1121.

Manuscript received: February 15, 2017
Accepted manuscript online: April 4, 2017
Version of record online: June 13, 2017